DOI: 10.1002/anie.201401059

Electron Tomography

# Three-Dimensional Characterization of Noble-Metal Nanoparticles and their Assemblies by Electron Tomography

*Sara Bals,* Bart Goris, Luis M. Liz-Marzán, and Gustaaf Van Tendeloo*

**Keywords:**
EDX · EELS · electron microscopy · electron tomography · metal nanoparticles

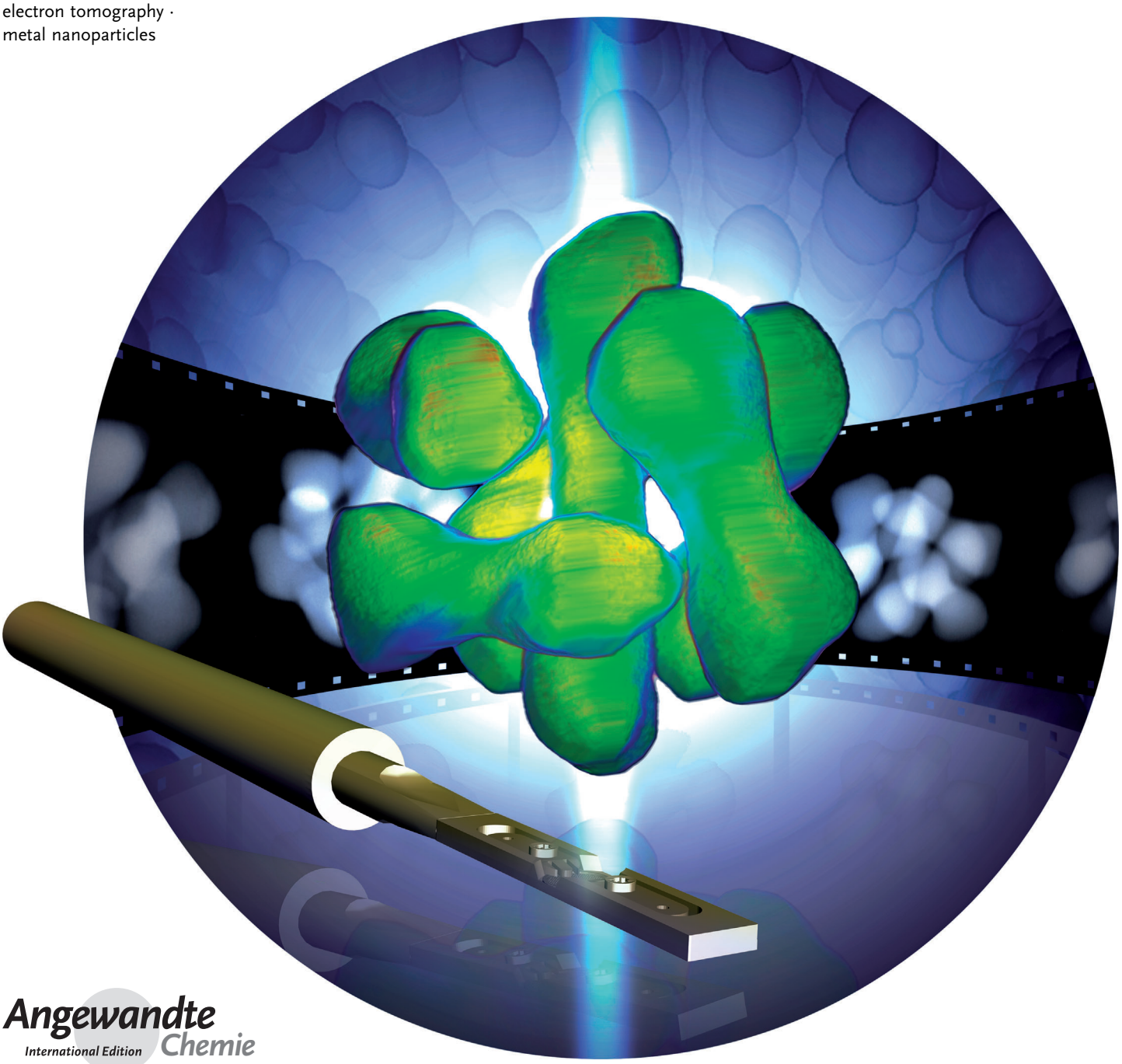

Angewandte International Edition Chemie

*New developments in the field of nanomaterials drive the need for quantitative characterization techniques that yield information down to the atomic scale. In this Review, we focus on the three-dimensional investigations of metal nanoparticles and their assemblies by electron tomography. This technique has become a versatile tool to understand the connection between the properties and structure or composition of nanomaterials. The different steps of an electron tomography experiment are discussed and we show how quantitative three-dimensional information can be obtained even at the atomic scale.*

**From the Contents**



## 1. Introduction

Nanoscience is currently considered a scientific field in its own right. However, it is a field that branches out into many of the "traditional" scientific fields, including chemistry, physics, biology, or materials science. Therefore, advances in nanoscience are unavoidably linked to developments in synthetic and theoretical methods, as well as characterization techniques.[1] In the context of "chemical nanoscience", crucial challenges are related to understanding the growth mechanisms of nanoparticles,[2] as well as their mutual interactions and self-assembly processes.[3] In both cases, a variety of characterization tools are required, which provide complementary information. These needs have boosted the tremendous development of electron microscopy and indeed a huge amount of information can be obtained from currently available electron microscopes.

In particular, transmission electron microscopy (TEM) and scanning transmission electron microscopy (STEM) are excellent techniques to investigate nanomaterials. Not only structural, but also chemical and even electronic information can nowadays be obtained, atomic column by atomic column.[4] However, TEM and most related techniques actually provide only a two-dimensional (2D) projection of what is a three-dimensional (3D) object. To overcome this problem, 3D electron microscopy or so-called "electron tomography" has been developed.[5] Most results have been achieved at the nanometer level, but recent developments have pushed the resolution of the technique to the atomic level.[6] In addition to 3D structural information, chemical composition can be investigated in 3D by combining the concepts of tomography with analytical TEM techniques.[7] In this manner, electron tomography has become a versatile tool to understand the connection between the properties and structure or composition of nanomaterials.[8]

Herein we focus on the possibility of using TEM to obtain 3D information from nanomaterials. Although electron tomography has been long used in biology, the resolution requirements for nanomaterials characterization have promoted impressive developments, such as atomic resolution or chemical information in 3D. There is a wide variety of nanomaterials, however, for several reasons we focus on metal nanoparticles and their assemblies. First of all, metal nanoparticles have generated a tremendous interest because of their excellent performance in plasmonics and catalysis,[9] as well as in other fields, in which their performance is strongly determined by a strict control of morphology and composition. Therefore, controlling the size, shape, and elemental distribution in (multi)-metallic nanostructures requires detailed information in 3D, with sufficient spatial resolution. In the case of catalytic nanoparticles, their activity is closely related to the crystallographic nature of the surface facets, on which reactants can adsorb, as well as to the presence of crystallographic defects, such as twin planes or dislocations. Therefore, atomic resolution is necessary for a complete picture of the system. Additionally, the applications of metal nanoparticles in plasmonics rely on the unusual inhomogeneous enhancement of electromagnetic fields within and around the nanoparticles. The use of electron microscopy and electron tomography toward understanding the plasmonic response of metal nanoparticles not only relies on the capability to provide detailed morphological information, but even on the possibility of exciting plasmon modes in situ, and obtaining (even three-dimensional) maps of field distributions.

## 2. Electron Tomography

### 2.1. History

Electron tomography has been applied in the biological sciences since the 1970s, but the resolution in this case is typically limited to the nanometer range because of several parameters, such as beam damage, the thickness of the sample, and sample preparation. For inorganic materials, beam damage is less important though it might still be a bottleneck for specific samples, but there are more important problems to overcome. Conventional bright-field TEM (BF-TEM) images of crystalline materials are often dominated by Bragg scattering and for certain orientations, the interaction is nonlinear. This violates the so-called "projection requirement", which states that each image of a tilt series for electron tomography should be a monotonic

[*] Prof. Dr. S. Bals, Dr. B. Goris, Prof. Dr. G. Van Tendeloo
Electron Microscopy for Materials Research (EMAT), University of Antwerp
Groenenborgerlaan 171, B-2020, Antwerp (Belgium)
E-mail: Sara.Bals@uantwerpen.be
Prof. Dr. L. M. Liz-Marzán
Bionanoplasmonics Laboratory, CIC biomaGUNE
Paseo de Miramón 182, 20009 Donostia-San Sebastian (Spain)
and
Ikerbasque, Basque Foundation for Science, 48011 Bilbao (Spain)

  

projection of a physical property of the sample under investigation.[10] Therefore, it was only in the past 15 years that electron tomography has been introduced in materials science. One of the earliest studies demonstrating bright-field (BF) tomography for the reconstruction of porous zeolites was published by Koster et al.[11] However, the presence of diffraction contrast in BF-TEM images of crystalline materials hampered the application of the technique to metallic nanostructures. The development of electron tomography based on high-angle annular dark-field (HAADF) STEM images however led to the possibility of characterizing crystalline nanoparticles in 3D as well.[5,12] Ever since, this technique has been used in a wide variety of studies where both two-dimensional, one-dimensional, and zero-dimensional nanostructures have been investigated.[13]

Over the years, different electron-microscopy techniques, such as BF-TEM, HAADF-STEM, annular dark-field TEM, electron holography, and energy-filtered TEM (EFTEM), have all been extended to 3D, providing a world of new information on structure–function relationships across a broad range of samples and applications.[5,7,14] For many years, the ultimate goal has been to achieve electron tomography with atomic resolution, since this would even further increase the potential for nanomaterials characterization. Although this is not yet a standard possibility for all types of samples, significant progress has recently been achieved using different approaches, which will be further discussed herein. Lately, electron tomography is often combined with an additional dimension, such as time or temperature of the specimen, thereby enabling 4D characterization.[15] In this manner, physical properties, such as the thermal stability of nanostructures can be investigated as well.[16]

### 2.2. Principles of the Technique

When applying conventional electron tomography, a tilt series of projection images is acquired by tilting the sample in the TEM over a large tilt angle range, with a tilt increment of typically 1° or 2° (See Scheme 1 a,b). Next, this so-called tilt series of projection images is aligned, using for example, cross-correlation. Through a mathematical algorithm, the tilt series is combined into a 3D reconstruction of the original object (see Scheme 1 c). When using "direct back-projection",[17] the images of the tilt series are back-projected along the original acquisition angles. It is hereby assumed that the projection requirement is fulfilled.

3D reconstructions obtained by direct back-projection appear blurred as a result of an uneven sampling of the spatial frequencies. Therefore, a weighting filter is applied, resulting in a technique that is referred to as "weighted back-projection" and which is the most commonly used reconstruction algorithm. With the increase of computing power, also iterative reconstruction techniques, such as for example, the simultaneous iterative reconstruction technique (SIRT) have become widely used.[18] These algorithms iteratively improve the quality of the reconstruction by minimizing the difference between the original projection images and forward projections of the intermediate reconstructions. Currently, the quality of the reconstruction is predominantly determined by the number of projection images. In practice,

*Sara Bals received her Ph.D. from the University of Antwerp in 2003in the group of Prof. G. Van Tendeloo. From 2003–2004, she joined NCEM at the Lawrence Berkeley National Laboratory. Currently she is a Professor at EMAT, the electron microscopy group at the University of Antwerp. Her main research interest consists of the application and further development of electron tomography for advanced nanostructured materials. In 2013 she received an ERC Starting Grant.*

*Luis M. Liz-Marzán has a Ph.D. from the University of Santiago de Compostela (1992) in the group of Prof. Arturo López-Quintela and has been a postdoc at Utrecht University and (more recently) visiting professor at various universities and research centers. He has been a Professor in Physical Chemistry at the University of Vigo (1995–2012), and is currently an Ikerbasque Research Professor and Scientific Director of CIC biomaGUNE in San Sebastián. His interests include nanoparticle synthesis and assembly, nanoplasmonics, and development of nanoparticle-based sensing and diagnostic tools. He received an ERC Advanced Grant in 2011.*

*Bart Goris received his Ph.D. from the University of Antwerp in 2014 in the group of Prof. G. Van Tendeloo under the supervision of Prof. S. Bals. His main interests are electron microscopy, electron tomography and their applications both on the nanometer and the atomic scale.*

*Gustaaf Van Tendeloo graduated from the University of Antwerp in 1974. Currently, he is a Professor at the University of Antwerp and part-time professor at the University of Brussels. His research focus is on the application of electron microscopy to different aspects of materials science. He is the leader of the electron microscopy group EMAT and director of the Nano Center of Excellence of the University. In 2009, he received an ERC Advanced Grant.*

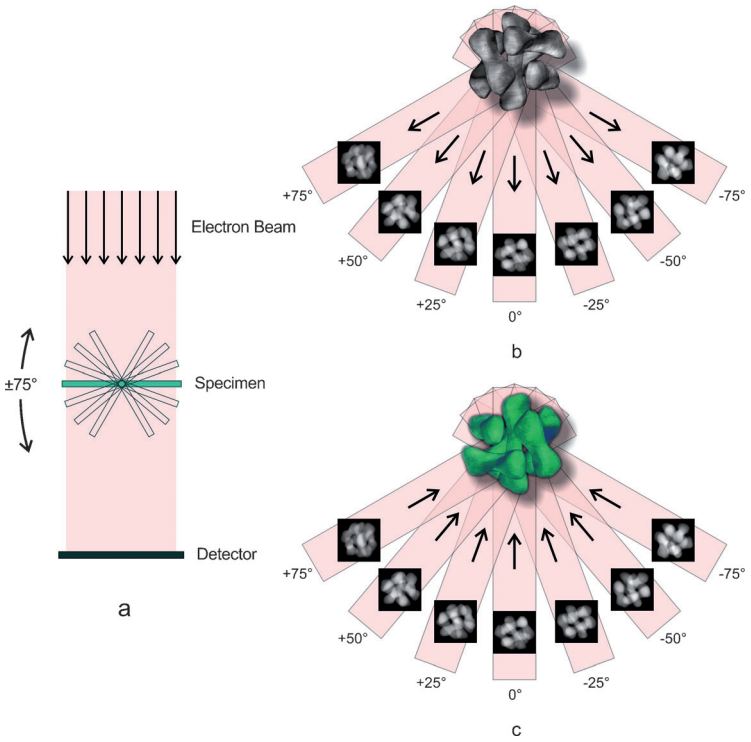


***Scheme 1.*** Illustration of a continuous electron tomography experiment, including the acquisition of a tilt series (a,b) and back-projection of the images along their original acquisition directions (c).

this number is determined by the stability of the sample under the electron beam and by geometrical constraints. It is indeed often impossible to tilt the sample over the full 360°, owing to the limited space for the sample holder in between the objective pole pieces of the microscope or because of shadowing effects that occur at higher tilt angles. These limits lead to a so-called "missing wedge" of projection images. The lack of projections results in different artifacts in the 3D reconstruction, among which an elongation in the direction along the missing wedge is the most prominent one. To overcome this problem and to minimize missing-wedge artifacts, dedicated experiments are performed, such as, dual tilt axis tomography, where the missing wedge of information is reduced to a missing pyramid.[19] In such experiments, two tilt series are acquired along two corresponding tilt axes that are perpendicular to each other. An approach to eliminate the missing wedge completely is provided by "on-axis tomography". In this case, a needle shaped sample is attached at the end of a dedicated on-axis tomography holder enabling a 360° tilt in the electron microscope.[20] Such needle-shaped samples can be prepared by focused-ion-beam milling, but mostly bulk materials are investigated in this manner. Nevertheless, in recent studies the technique was also applied to image nanoparticles in 3D, but sample preparation is far from straightforward.[21] Despite the possible presence of certain artifacts, it is still safe to state that electron tomography has evolved into a standard tool to visualize the morphology of nanostructures on a routine basis.

### *2.3. Quantification in 3D*

The demand in the field of electron tomography is nowadays increasingly focused towards quantitative measurements of properties such as morphologies or chemical compositions. Approaches in which the missing wedge is minimized can be thought of as a crucial step towards quantification in 3D,[20a,22] but as discussed above these are not always applicable to the 3D investigation of nanoparticles. An additional problem is that extracting quantitative data from a 3D reconstruction requires a segmentation step to determine the correspondence between different grayscales in the reconstruction and different compositions in the original structure. Segmentation is generally performed manually but this approach is very time consuming and more importantly, it includes a subjective component. Automatic segmentation based on a threshold at different gray levels might be a solution to this problem, but (missing-wedge) artifacts can hamper this procedure. It has been found that samples must be tilted over a range of at least $\pm 80°$ to obtain reliable quantitative measurements.[20a,23] Even if projection images could be acquired from a full range of angles, several other types of artifacts, such as the effect of limited sampling and slight misalignments, might still be present and will hamper the segmentation step. A quantitative interpretation based on the conventional 3D reconstruction algorithms is therefore quite difficult. It must be noted that none of the conventional reconstruction algorithms, such as weighted back-projection and SIRT, uses additional information on the system that is to be reconstructed. By using other information, the quality of a reconstruction can be drastically improved and very often, such additional information on the sample is indeed available or can be obtained using other (TEM) techniques. One approach to incorporate existing knowledge is the so-called "discrete tomography", as implemented in the discrete algebraic reconstruction algorithm (DART). DART is an iterative algorithm that alternates between steps of the SIRT algorithm from continuous tomography and certain discretization steps.[13b,24] Both for BF-TEM and HAADF-STEM tomography it has been shown that missing-wedge artifacts are significantly reduced.[13b,25] Another important advantage is that segmentation of the 3D data set is carried out during the reconstruction in a reliable and objective manner.[23] Results showed that it is possible to obtain reliable and quantitative results using the DART algorithm, even for a tilt range as limited as $\pm 60°$.[23] A different kind of prior knowledge is exploited when using compressive sensing based reconstruction algorithms.[26] A specific variant of this approach is referred to as "total variation minimization" (TVM), where it is assumed that the object to be reconstructed has a sparse gradient at the nanometer scale. For nanoscale objects, it is indeed often a good assumption that boundaries between different compounds are sharp, leading to a sparse gradient of the object. Similar to DART, TVM has the advantage that the resulting 3D reconstructions suffer less

  

from the missing wedge. Clearly both DART and TVM are very promising algorithms when quantitative measurements in 3D are required. This is especially the case for experiments in which the missing wedge cannot be avoided, such as 3D reconstructions of nanoparticles. In a recent study, a combination of TVM and DART was proposed, in which the threshold intensities from a TVM reconstruction serve as the input gray values for a discrete reconstruction.[27] This approach leads to straightforward segmentation and therefore quantification of the reconstruction. A comparison between SIRT (Figure 1 a), TVM (Figure 1 b), and DART (Figure 1 c) reconstructions of Au nanoparticles is presented in Figure 1. Slices through the TVM reconstruction (Figure 1 e,h) reveal that the boundary facets of the nanoparticles are easier to determine from this reconstruction than from the SIRT reconstruction (Figure 1 d,g). The DART reconstruction (Figure 1 f,i) has the advantage that segmentation and quantification become much more straightforward since thresholding is already applied during the algorithm.

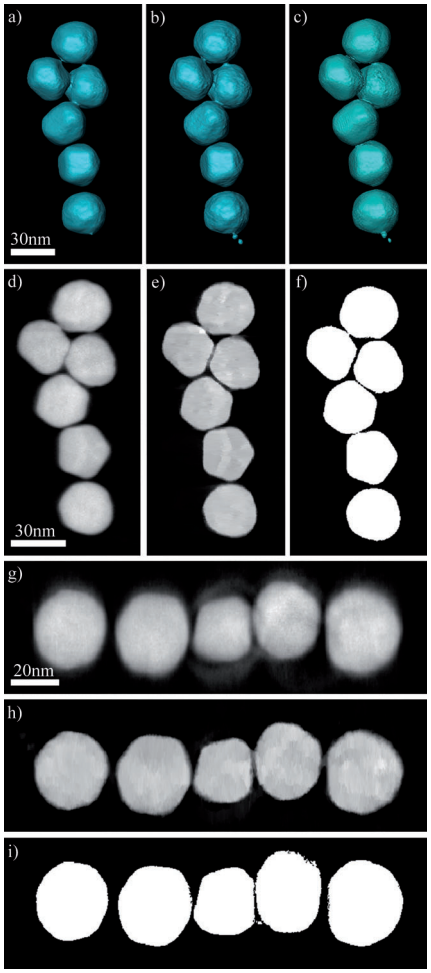


***Figure 1.*** Reconstruction of gold nanoparticles with a diameter of approximately 30 nm. Isosurface renderings of a) SIRT, b) TVM, and c) DART reconstructions, respectively. d,g) From the slices through the SIRT reconstruction, it can be seen that an elongation along the direction of the missing wedge is present. This elongation is less pronounced when inspecting the slices through the TVM (e,h) or DART (f,i) reconstructions.

### *2.4. Electron Tomography for Nanoparticles*

Electron tomography has become a standard characterization technique in the study of a broad variety of nanostructures. Given the aperiodic nature of the nanoparticles, it is of great importance to investigate their structure and composition in 3D. Very often, questions that need to be answered are related to particle size distribution, surface (facets) characterization, particle distribution in a matrix material, or interface investigation in the case of heteronanoparticles that consist of more than one material with different compositions. In most studies to date, conventional electron tomography with a resolution in the nanometer range was applied, but current demands in materials science push the need for atomic-resolution electron tomography as well.

Since its earliest use, the combination of HAADF-STEM imaging and electron tomography has been used in a variety of studies where a 3D characterization of crystalline structures at the nanometer scale is required. One of the first examples in which the 3D morphology of nanoparticles was studied, was the demonstration that magnetotactic bacteria contain $Fe_3O_4$ magnetite nanocrystals exhibiting six {110} lateral facets.[5] A similar study, but applied to isolated nanoparticles, was performed for $Mn_3O_4$ octahedral nanoparticles[28] and Pd nanoparticles exhibiting a more complex morphology.[29] In combination with high resolution STEM projections, the technique was also used to characterize the morphology of single-crystalline Au nanoparticles with a twisted shape.[13a]

Besides the study of the morphology of 0D nanostructures, their distribution inside a matrix can also be observed using electron tomography. A first example is a heterogeneous catalyst where small $Pd_6Ru_6$ particles were embedded in a mesoporous silica support. Using tomographic reconstructions, it was shown that the particles were truly located inside the hexagonal mesopores.[5] Other examples where the presence of nanoparticles inside a mesoporous material were investigated include the study of Au particles in an Au/SBA-15 model catalyst particle[30] or the study of $TiO_2$ nanoparticles in a $TiO_2/SiO_2$ mesoporous photocatalyst.[31] The 3D structure of the porous materials themselves has also been the subject of several electron tomography studies.[8f,14a,22a,32]

### *2.5. Electron Tomography of Nanoparticle Assemblies*

During recent years, assemblies of nanoparticles in both two and three dimensions have gained increasing attention owing to their improved properties compared to those of their building blocks.[3b,c,13d,33] By varying the size, the shape of the nanoparticles, and their surface chemistry, assemblies with unique configurations can be obtained. Owing to the complex 3D nature of such assemblies, 2D imaging is not sufficient and 3D characterization by electron tomography has become a prerequisite.[13c,d] A clear example is provided in Figure 2, where an assembly of Au nanodumbbells capped with polystyrene chains is shown. Such assemblies may have

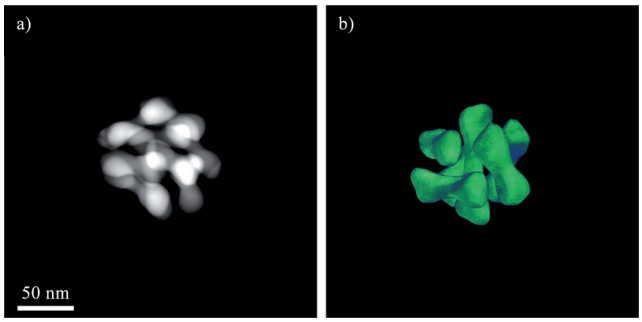


***Figure 2.*** a) 2D HAADF-STEM image of an assembly of Au nanodumbbells. By applying electron tomography, as shown in (b), the full 3D structure can be interpreted from the reconstructed image.

applications in the field of plasmonics and metamaterials, but their properties can only be understood if the dimensions and mutual orientations are known in detail. It is clear that only from 3D HAADF-STEM reconstructions (Figure 2b), it is possible to interpret the complete 3D structure of these complex assemblies. The reconstruction provides important information, not only about each of the particles, but also about the mutual orientation of the nanodumbbells within the assembly.

Several groups have demonstrated the ability to investigate nanoparticle assemblies by electron tomography.[13c,d,33a] In these studies, conventional approaches toward acquisition and reconstruction were used to obtain the data. However, to extract quantitative information, optimization of the electron tomography experiment is required. This is especially the case for large assemblies that have a thickness of over 500 nm. For such systems, the conventional approaches yield different types of artifacts hampering a quantitative interpretation of the 3D data. The problem is related to the so-called "cupping artifact",[34] which is due to the thickness of the assembly and the high atomic number of Au. This results in an increase of multiple scattering and backscattering. Consequently, only part of the incoming electron beam is scattered towards the detector, leading to an underestimation of the intensity. The cupping artifact clearly affects the reconstruction of the particles at the inner shells of this assembly. As a consequence, both qualitative and quantitative interpretations of the results are no longer straightforward. In particular, quantitative interpretation will be hampered: when quantifying a 3D reconstruction, a segmentation step is needed as explained in Section 2.3. As a result of the cupping artifact, the nanoparticles at the inner part of the assembly will have a different gray level from those at the outside, thereby complicating the segmentation and therefore the quantification of the results.

In a recent study, an improved route towards the quantitative structure determination of large (400–500 nm) 3D assemblies of Au nanoparticles was proposed, which required optimization of both the acquisition technique and the reconstruction algorithm.[35] By combining incoherent bright-field (IBF) STEM with TVM, three-dimensional data could be obtained without any information loss. IBF-STEM has been successfully used for electron tomography of thick samples.[36] Since the IBF-STEM signal is considered to be incoherent, it scales with the atomic number $Z$ of the elements present in the sample and the thickness of the sample. In Figure 3, it is shown that the use of IBF-STEM indeed enables the particles located at the inner part of an

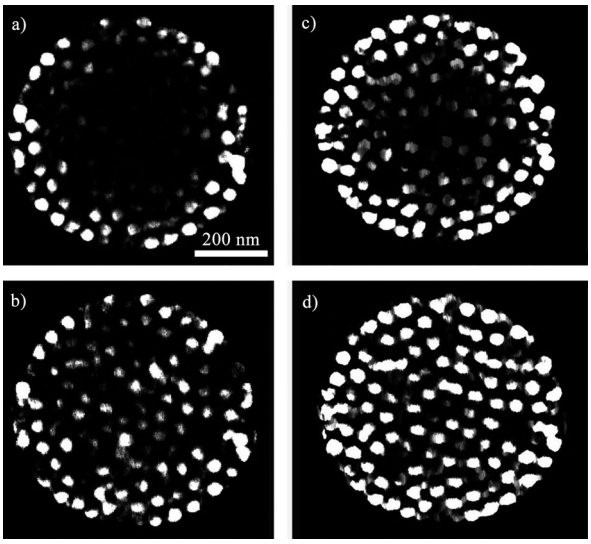


***Figure 3.*** a,b) Slices through the reconstructed volumes based on a tilt series acquired by HAADF-STEM or IBF-STEM combined with a SIRT reconstruction. A significant improvement is observed for the result obtained through IBF-STEM. c,d) Applying TVM during the reconstruction is also beneficial. d) When combining IBF-STEM and TVM, an optimal result is obtained.

assembly to be better detected. However, when a SIRT reconstruction was used, not all the particles could be identified. Only through combination of IBF-STEM with TVM could a full characterization and quantification be achieved. For example, in this case we were able to determine the number of particles in each reconstruction. In case a segmentation (using the same threshold value) was performed for the HAADF-STEM series, reconstructed using SIRT, a total number of 70 segmented particles was found. When segmenting the series acquired by IBF-STEM and reconstructing using TVM the total number of segmented particles equaled 302. It must be pointed out that these 3D investigations can be combined with theoretical and quantitative calculations, leading to an improved understanding concerning the growth of these structures. Such understanding may enable a more efficient synthesis of 3D assemblies.[37]

### *2.6. Electron Tomography at the Atomic Scale*

Achieving atomic resolution in 3D has been the ultimate dream in the field of electron tomography for many years. It was shown recently that electron tomography can be extended to atomic resolution and that 3D reconstructions at the atomic scale can be achieved using different approaches.[6a,c,e–g,38] 3D reconstructions with atomic resolution can even be obtained from a limited number of high-resolution

  

HAADF-STEM images, using advanced statistical parameter estimation and so-called discrete tomography.[6a,f,39] The approach is currently based on the assumption that all atom positions are fixed on a grid and this has been shown to be a good starting point to obtain unique insights concerning the structure and the formation of nanoparticles. A different approach was proposed by Scott et al. where an equally sloped tomography (EST) technique was applied to create a 3D reconstruction of an Au nanoparticle with a resolution of 2.4 Å.[6e] Although not all atoms could be located in this reconstruction, it was concluded that individual atoms could be observed in some parts of the nanoparticle. The same technique has also been combined with a post-filtering technique to obtain a reconstruction of the atoms around a dislocation in a Pt nanocrystal.[6c] Although these are promising results, the above mentioned techniques have the disadvantage that either many high-resolution STEM projections are required, leading to increased damage of the samples, or it is assumed that atoms are positioned on a regular grid. However, many particle properties are exactly determined by small deviations from such a perfect grid. To make it worse, it is challenging to acquire a large number of projection images from a single nanoparticle without changing its (surface) structure.

As an alternative to the approaches mentioned above, compressive sensing based electron tomography was applied. Compressive sensing (CS) is a technique specialized in finding a solution that has a sparse representation to a set of linear equations.[40] At the atomic scale, the approach exploits the sparsity of the object since most of the voxels that need to be reconstructed correspond to vacuum and only a limited number of voxels are occupied by atoms. Using this idea in a tomographic reconstruction algorithm will result in a more reliable atomic-scale reconstruction than with reconstructions based on conventional algorithms. An additional important advantage is that, just a few projection images are sufficient for a reliable reconstruction. Mathematically, the sparsity is introduced in the reconstruction process with a regularization parameter λ [Eq. (1)].

$$\hat{x} = \arg\min_{x} \left[ \|Ax - b\|_2^2 + \lambda \|x\|_1 \right] \quad (1)$$

In Equation (1), the first term represents the correspondence of the reconstructed object $x$ with the projections $b$ and the second term ensures the sparsity of the final solution. This approach has been applied to reconstruct the structure of Au nanorods.[6d] Such reconstructions enable the influence of the synthesis method on the final morphology of Au nanorods to be investigated. The result of such a reconstruction is shown in Figure 4a, where atomic resolution allows it to be seen that the surface facets of this Au nanorod are mainly composed of {110} and {100} facets. However, when inspecting 3D reconstructions of nanorods that were synthesized using a different surfactant, it was determined that {520} facets were the most dominant ones (Figure 4b).

During the reconstruction process, no prior knowledge about the atomic lattice was used. As a result, small deviations of the positions of the atoms from a perfect lattice can be measured. This means that surface strain can be measured when applying a 3D extension of the geometrical phase analysis (GPA) to the 3D reconstruction by selecting three reflections from its Fourier transform.[41] The result is a 3D strain field of which the $\varepsilon_{zz}$ component of the Au nanorod from Figure 4a is shown in Figure 4c. All measured strain fields are relative to a reference region which is selected in the middle of the Au nanorod, which is assumed to yield an undistorted lattice. From these measurements, it is clear that the tip of the nanorod is (approximately) 3% strained, which is important for a thorough understanding of the catalytic and optical properties of these nanorods.

Going further than simply determining the positions of atoms, a crucial aim is also identifying the atom type of individual atoms in bimetallic nanoparticles.[42] Such particles often provide novel properties in comparison to their monometallic counterparts. To understand these properties, a complete 3D characterization is often required where the exact positioning of the different chemical elements is crucial, especially at interfaces. This chemical information can be obtained from HAADF-STEM tomography owing to the dependence of the intensity in the projection images on the atomic number. In principle, identification of the chemical nature of the atoms becomes possible on the basis of a quantitative comparison of the intensities of the different voxels in the final 3D reconstruction. Therefore, a parametric

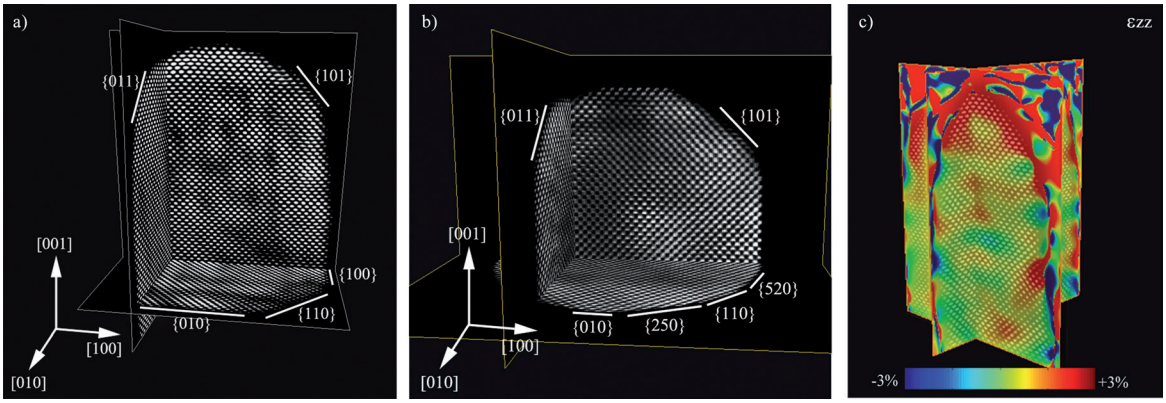


***Figure 4.*** Atomic scale reconstruction of Au nanorods. a,b) Orthogonal slices through the atomic scale reconstruction of Au nanorods prepared using different surfactants. The side facets of these rods can be clearly recognized. c) Strain measurement along the major axis of the nanorod.

model in which projection images of the atomic columns are described using Gaussian peaks has been assumed. The outcome of the statistical parameter estimation was used as an input for the CS algorithm described above in Equation (1). A detailed analysis of the position and the atom type in a core–shell bimetallic nanorod was performed using orthogonal slices through the 3D reconstruction, as shown in Figure 5. Individual Ag and Au atoms can be distinguished, even at the metal–metal interface, by comparing their relative intensities. An intensity profile was acquired along the direction indicated by the white rectangular box in Figure 5b and shown in Figure 5f it is clear that Au and Ag atoms can indeed be identified from their intensities using a threshold value. In this manner, each atom in the cross-sections shown in Figure 5b,c was assigned to be either Ag or Au. The result is shown in Figure 5d,e and leads to correct indexing of the type of interfacial planes.

## 3. Outlook

### 3.1. Use of EDX Tomography

Energy dispersive X-ray (EDX) spectroscopy is an analytical TEM technique. The specific energies of the generated X-rays during the interaction between the electrons and the sample are characteristic for the chemical elements that are present in the specimen and can be used for a chemical characterization. When combining STEM with X-ray spectroscopy analysis, a complete 2D mapping of the chemical elements in the specimen can be obtained. Since the number of generated X-rays scales with the thickness of the sample, such a 2D elemental map can in principle serve as a projection image for electron tomography. Pioneering work was performed by Möbus et al.[7] However, early attempts to obtain 3D information by EDX were complicated because of the directionality and inefficiency of the sample-detector geometry, since the EDX detector is typically placed under a specific tilt angle of the specimen. The optimal signal is then collected when the sample is tilted towards the detector and shadowing may block the signal at different tilt angles. As a result, EDX tomography results could only be obtained for specific needle-shaped samples where shadowing effects during the acquisition are avoided.[43] Recently, a new detector geometry has been developed where four X-ray detectors are placed symmetrically around the sample, thereby reducing the blocking of the generated X-rays.[44] Using this method, Genc et al. reported 3D EDX tomography for submicron oxide nanoparticles, but it remains far from straightforward to achieve 3D EDX results for smaller nanoparticles.[45] EDX tomography would be of particular interest to study the distribution of atoms in bimetallic nanoparticles (core–shell or alloys), since it determines their specific optical response or their catalytic activity.[46] An example of such a reconstruction is shown in Figure 6, where a 2D EDX map (Figure 6a) and a 3D EDX reconstruction (Figure 6b) of a Au@Ag nanocube are presented. The contrast in the 3D EDX reconstruction, based on the chemical difference in the core–shell structure, clearly

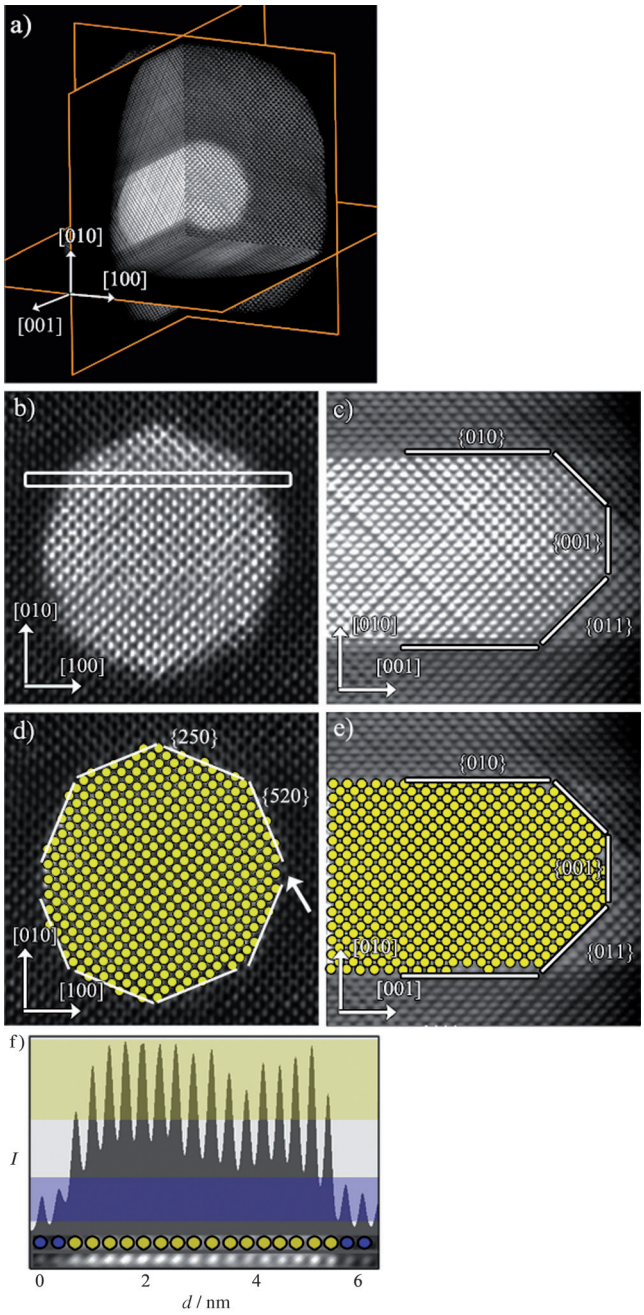


***Figure 5.*** Atomic resolution tomography of Au@Ag nanorods. a) Three orthogonal slices through the reconstruction show the core–shell structure of the nanorod. The atomic lattice can be resolved in all three slices. b,c) Detailed view of slices through the reconstruction perpendicular to and parallel to the major axis of the nanorod. In (c) artifacts are related to (currently) unavoidable sample drift during scanning, remaining scanning noise, and the acquisition geometry. f) An intensity profile was acquired along the direction indicated by the white rectangle in (b). d,e) Slices corresponding to (b) and (c), in which each Au atom is indicated by a yellow circle. The correct interfacial planes can be determined on the basis of intensity profiles through the reconstruction.

shows that the core of the particle has an octahedral shape. Additionally, many chemical transformations in nanoparticles involve morphological changes in 3D, so standard TEM

  

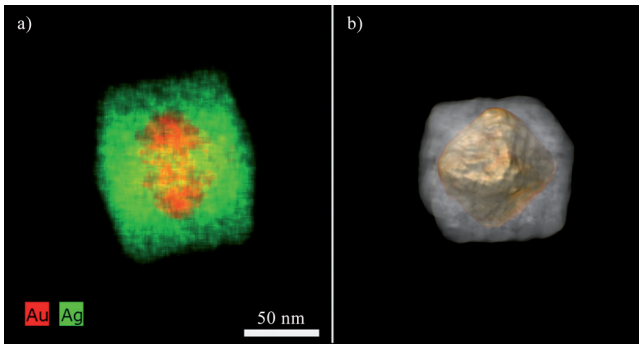


***Figure 6.*** a) 2D EDX map of a Au@Ag nanocube. Based on a tilt series of such 2D EDX maps the 3D reconstruction presented in (b) was obtained. The contrast in the 3D reconstruction is based on differences in chemical composition and it is clear that the core of the particle has an octahedral form.

analysis is typically insufficient to obtain a complete picture of the transformation and the corresponding mechanism. A characteristic example would be Galvanic replacement, by which solid metal nanoparticles become hollow through oxidation of one metal by another with a larger reduction potential, so that the metal with the larger reduction potential gets deposited in the form of so-called nanocages.[47] This example clearly illustrates the potential of 3D EDX mapping, but care needs to be taken when extracting quantitative information from such reconstructions. To reach this goal, the different steps of an EDX tomography experiment need to be optimized.

### *3.2. 3D Plasmon Mapping*

Localized surface plasmon resonances (LSPRs) are collective excitations of the conduction electrons that arise at the surface of metallic particles when irradiated by electromagnetic radiation. The occurrence of such surface plasmons has a large influence on the optical properties and potential applications of the nanoparticles, and knowledge of their spatial distribution is therefore crucial to understand the behavior of the nanostructures. Although LSPRs have typically been associated with illumination by light, it has been shown that electron beams can also be used to excite them. A modern plasmon-mapping technique is based on monochromated STEM electron energy loss spectroscopy (EELS), where a high spatial resolution can be combined with a high energy resolution.[48] Although for certain (highly symmetric) nanoparticle morphologies such 2D mapping provides sufficient information, a full analysis of more complicated morphologies requires additional detail. Hohenester and co-workers have recently shown theoretically that plasmon maps obtained by EELS can be used to create a 3D reconstruction of the plasmon fields surrounding a metallic nanoparticle.[49] Subsequently, Midgley et al. provided an experimental example where they present the three-dimensional imaging of LSPR modes for an Ag nanocube.[50] To obtain this result, they combined monochromated STEM EELS with non-negative matrix factorization and compressive sensing-based electron tomography. It is expected that more results will follow in the future resulting in a better understanding of the optical response of metallic nanoparticles.

*We would like to thank the colleagues who have contributed to this work over the years, including T. Altantzis, K. J. Batenburg, A. De Backer, Cristina Fernández-López, Sergio Gomez-Graña, Marek Grzelczak, H. Heidari, Ana Sánchez-Iglesias S. Van Aert and W. Van den Broek. We acknowledge financial support from European Research Council (ERC Advanced Grant no. 267867- PLASMAQUO, ERC Advanced Grant no. 24691-COUNTATOMS, ERC Starting Grant no. 335078-COLOURATOMS), and also from the European Union under the Seventh Framework Program (Integrated Infrastructure Initiative N. 262348 European Soft Matter Infrastructure, ESMI). The work was also supported by the Flemish Fund for Scientific Research (FWO Vlaanderen) through a Ph.D. research grant to B.G..*

Received: January 31, 2014
Published online: August 11, 2014

[1] B. Pelaz, S. Jaber, D. J. de Aberasturi, V. Wulf, T. Aida, J. M. de La Fuente, J. Feldmann, H. E. Gaub, L. Josephson, C. R. Kagan, N. A. Kotov, L. M. Liz-Marzan, H. Mattoussi, P. Mulvaney, C. B. Murray, A. L. Rogach, P. S. Weiss, I. Willner, W. J. Parak, *ACS Nano* **2012**, *6*, 8468 – 8483.

[2] a) Y. N. Xia, Y. J. Xiong, B. Lim, S. E. Skrabalak, *Angew. Chem.* **2009**, *121*, 62 – 108; *Angew. Chem. Int. Ed.* **2009**, *48*, 60 – 103; b) F. Wang, V. N. Richards, S. P. Shields, W. E. Buhro, *Chem. Mater.* **2014**, *26*, 5 – 21; c) S. E. Lohse, N. D. Burrows, L. Scarabelli, L. M. Liz-Marzán, C. J. Murphy, *Chem. Mater.* **2014**, *26*, 34 – 43; d) M. Grzelczak, J. Perez-Juste, P. Mulvaney, L. M. Liz-Marzan, *Chem. Soc. Rev.* **2008**, *37*, 1783 – 1791.

[3] a) Z. Y. Tang, N. A. Kotov, *Adv. Mater.* **2005**, *17*, 951 – 962; b) E. V. Shevchenko, D. V. Talapin, N. A. Kotov, S. O'Brien, C. B. Murray, *Nature* **2006**, *439*, 55 – 59; c) M. Grzelczak, J. Vermant, E. M. Furst, L. M. Liz-Marzan, *ACS Nano* **2010**, *4*, 3591 – 3605.

[4] a) D. A. Muller, *Nat. Mater.* **2009**, *8*, 263 – 270; b) K. W. Urban, *Nat. Mater.* **2009**, *8*, 260 – 262.

[5] P. A. Midgley, M. Weyland, *Ultramicroscopy* **2003**, *96*, 413 – 431.

[6] a) S. Bals, M. Casavola, M. A. van Huis, S. Van Aert, K. J. Batenburg, G. Van Tendeloo, D. Vanmaekelbergh, *Nano Lett.* **2011**, *11*, 3420 – 3424; b) S. Bals, S. Van Aert, C. P. Romero, K. Lauwaet, M. J. Van Bael, B. Schoeters, B. Partoens, E. Yucelen, P. Lievens, G. Van Tendeloo, *Nat. Commun.* **2012**, *3*, 897; c) C. C. Chen, C. Zhu, E. R. White, C. Y. Chiu, M. C. Scott, B. C. Regan, L. D. Marks, Y. Huang, J. Miao, *Nature* **2013**, *496*, 74 – 77; d) B. Goris, S. Bals, W. Van den Broek, E. Carbo-Argibay, S. Gomez-Grana, L. M. Liz-Marzan, G. Van Tendeloo, *Nat. Mater.* **2012**, *11*, 930 – 935; e) M. C. Scott, C. C. Chen, M. Mecklenburg, C. Zhu, R. Xu, P. Ercius, U. Dahmen, B. C. Regan, J. W. Miao, *Nature* **2012**, *483*, 444 – 447; f) S. Van Aert, K. J. Batenburg, M. D. Rossell, R. Erni, G. Van Tendeloo, *Nature* **2011**, *470*, 374 – 377; g) D. Van Dyck, F. R. Chen, *Nature* **2012**, *486*, 243 – 246.

[7] G. Möbus, R. C. Doole, B. J. Inkson, *Ultramicroscopy* **2003**, *96*, 433 – 451.

[8] a) S. Bals, S. Van Aert, G. Van Tendeloo, *Curr. Opin. Solid State Mater. Sci.* **2013**, *17*, 107 – 114; b) J. J. Fernandez, *Curr. Opin. Solid State Mater. Sci.* **2013**, *17*, 93 – 106; c) H. Jinnai, X. Jiang, *Curr. Opin. Solid State Mater. Sci.* **2013**, *17*, 135 – 142; d) P. A.

Midgley, Z. Saghi, *Curr. Opin. Solid State Mater. Sci.* **2013**, *17*, 89 – 92; e) D. Wolf, A. Lubk, F. Roder, H. Lichte, *Curr. Opin. Solid State Mater. Sci.* **2013**, *17*, 126 – 134; f) J. Zecevic, K. P. de Jong, P. E. de Jongh, *Curr. Opin. Solid State Mater. Sci.* **2013**, *17*, 115 – 125.

[9] a) A. Guerrero-Martínez, M. Grzelczak, L. M. Liz-Marzán, *ACS Nano* **2012**, *6*, 3655 – 3662; b) P. Hervés, M. Pérez-Lorenzo, L. M. Liz-Marzán, J. Dzubiella, Y. Lu, M. Ballauff, *Chem. Soc. Rev.* **2012**, *41*, 5577 – 5587.

[10] P. W. Hawkes in *Electron Tomography: Threedimensional imaging with the transmission electron microscope* (Ed.: J. Frank), Plenum, New York, London **1992**.

[11] A. J. Koster, U. Ziese, A. J. Verkleij, A. H. Janssen, K. P. de Jong, *J. Phys. Chem. B* **2000**, *104*, 9368 – 9370.

[12] P. A. Midgley, M. Weyland, J. M. Thomas, B. F. G. Johnson, *Chem. Commun.* **2001**, 907 – 908.

[13] a) P. C. Angelomé, H. H. Mezerji, B. Goris, I. Pastoriza-Santos, J. Pérez-Juste, S. Bals, L. M. Liz-Marzán, *Chem. Mater.* **2012**, *24*, 1393 – 1399; b) S. Bals, K. J. Batenburg, J. Verbeeck, J. Sijbers, G. Van Tendeloo, *Nano Lett.* **2007**, *7*, 3669 – 3674; c) M. P. Boneschanscher, W. H. Evers, W. K. Qi, J. D. Meeldijk, M. Dijkstra, D. Vanmaekelbergh, *Nano Lett.* **2013**, *13*, 1312 – 1316; d) H. Friedrich, C. J. Gommes, K. Overgaag, J. D. Meeldijk, W. H. Evers, B. de Nijs, M. P. Boneschanscher, P. E. de Jongh, A. J. Verkleij, K. P. de Jong, A. van Blaaderen, D. Vanmaekelbergh, *Nano Lett.* **2009**, *9*, 2719 – 2724; e) Z. He, X. Ke, S. Bals, G. Van Tendeloo, *Carbon* **2012**, *50*, 2524 – 2529; f) A. B. Hungría, D. Eder, A. H. Windle, P. A. Midgley, *Catal. Today* **2009**, *143*, 225 – 229; g) A. B. Hungría, B. H. Juárez, C. Klinke, H. Weller, P. A. Midgley, *Nano Res.* **2008**, *1*, 89 – 97; h) D. Rodríguez-Fernández, T. Altantzis, H. Heidari, S. Bals, L. M. Liz-Marzán, *Chem. Commun.* **2014**, *50*, 79 – 81; i) S. P. Sree, J. Dendooven, K. Masschaele, H. M. Hamed, S. Deng, S. Bals, C. Detavernier, J. A. Martens, *Nanoscale* **2013**, *5*, 5001 – 5008.

[14] a) S. Bals, K. J. Batenburg, D. Liang, O. Lebedev, G. Van Tendeloo, A. Aerts, J. A. Martens, C. E. Kirschhock, *J. Am. Chem. Soc.* **2009**, *131*, 4769 – 4773; b) S. Bals, G. Van Tendeloo, C. Kisielowski, *Adv. Mater.* **2006**, *18*, 892 – 895; c) B. Goris, S. Bals, W. Van den Broek, J. Verbeeck, G. Van Tendeloo, *Ultramicroscopy* **2011**, *111*, 1262 – 1267; d) U. Kaiser, A. Chuvilin, *Microsc. Microanal.* **2003**, *9*, 78 – 79; e) P. A. Midgley, R. E. Dunin-Borkowski, *Nat. Mater.* **2009**, *8*, 271 – 280; f) G. Möbus, B. J. Inkson, *Appl. Phys. Lett.* **2001**, *79*, 1369 – 1371; g) R. J. Spontak, J. C. Fung, M. B. Braunfeld, J. W. Sedat, D. A. Agard, A. Ashraf, S. D. Smith, *Macromolecules* **1996**, *29*, 2850 – 2856; h) A. C. Twitchett, R. E. Dunin-Borkowski, P. A. Midgley, *Phys. Rev. Lett.* **2002**, *88*, 238302; i) M. Weyland, P. A. Midgley, *Microsc. Microanal.* **2003**, *9*, 542 – 555; j) D. Wolf, A. Lubk, H. Lichte, H. Friedrich, *Ultramicroscopy* **2010**, *110*, 390 – 399.

[15] a) K. Jarausch, P. Thomas, D. N. Leonard, R. Twesten, C. R. Booth, *Ultramicroscopy* **2009**, *109*, 326 – 337; b) O. H. Kwon, A. H. Zewail, *Science* **2010**, *328*, 1668 – 1673; c) A. Zewail, J. M. Thomas, *4D electron microscopy*: *Imaging in space and time*, Imperial College Press, London, **2009**.

[16] B. Goris, M. A. Van Huis, S. Bals, H. W. Zandbergen, L. Manna, G. Van Tendeloo, *Small* **2012**, *8*, 937 – 942.

[17] a) W. Hoppe, R. Langer, G. Knesch, C. Poppe, *Naturwissenschaften* **1968**, *55*, 333 – 336; b) R. A. Crowther, D. J. Derosier, A. Klug, *Proc. R. Soc. London Ser. A* **1970**, *317*, 319 – 340.

[18] P. Gilbert, *J. Theor. Biol.* **1972**, *36*, 105 – 117.

[19] I. Arslan, J. R. Tong, P. A. Midgley, *Ultramicroscopy* **2006**, *106*, 994 – 1000.

[20] a) N. Kawase, M. Kato, H. Nishioka, H. Jinnai, *Ultramicroscopy* **2007**, *107*, 8 – 15; b) X. X. Ke, S. Bals, D. Cott, T. Hantschel, H. Bender, G. Van Tendeloo, *Microsc. Microanal.* **2010**, *16*, 210 – 217.

[21] K. Jarausch, D. N. Leonard, *J. Electron Microsc.* **2009**, *58*, 175 – 183.

[22] a) E. Biermans, L. Molina, K. Batenburg, S. Bals, G. Van Tendeloo, *Nano Lett.* **2010**, *10*, 5014 – 5019; b) see Ref.[20b].

[23] See Ref. [22a].

[24] K. J. Batenburg, S. Bals, J. Sijbers, C. Kubel, P. A. Midgley, J. C. Hernandez, U. Kaiser, E. R. Encina, E. A. Coronado, G. Van Tendeloo, *Ultramicroscopy* **2009**, *109*, 730 – 740.

[25] See Ref. [14a].

[26] a) Z. Saghi, D. J. Holland, R. Leary, A. Falqui, G. Bertoni, A. J. Sederman, L. F. Gladden, P. A. Midgley, *Nano Lett.* **2011**, *11*, 4666 – 4673; b) R. Leary, Z. Saghi, P. A. Midgley, D. J. Holland, *Ultramicroscopy* **2013**, *131*, 70 – 91; c) B. Goris, W. Van den Broek, K. J. Batenburg, H. H. Mezerji, S. Bals, *Ultramicroscopy* **2012**, *113*, 120 – 130.

[27] B. Goris, T. Roelandts, K. J. Batenburg, H. H. Mezerji, S. Bals, *Ultramicroscopy* **2013**, *127*, 40 – 47.

[28] Y. Li, H. Tan, X. Y. Yang, B. Goris, J. Verbeeck, S. Bals, P. Colson, R. Cloots, G. Van Tendeloo, B. L. Su, *Small* **2011**, *7*, 475 – 483.

[29] S. Benlekbir, T. Epicier, M. Bausach, M. Aouine, G. Berhault, *Philos. Mag. Lett.* **2009**, *89*, 145 – 153.

[30] U. Ziese, A. H. Janssen, J. L. Murk, W. J. C. Geerts, T. Van der Krift, A. J. Verkleij, A. J. Koster, *J. Microsc.* **2002**, *205*, 187 – 200.

[31] E. Beyers, E. Biermans, S. Ribbens, K. De Witte, M. Mertens, V. Meynen, S. Bals, G. Van Tendeloo, E. Vansant, P. Cool, *Appl. Catal. B* **2009**, *88*, 515 – 524.

[32] a) G. Prieto, J. Zecevic, H. Friedrich, K. P. de Jong, P. E. de Jongh, *Nat. Mater.* **2013**, *12*, 34 – 39; b) O. Ersen, J. Parmentier, L. A. Solovyov, M. Drillon, C. Pham-Huu, J. Werckmann, P. Schultz, *J. Am. Chem. Soc.* **2008**, *130*, 16800 – 16806; c) J. Dendooven, B. Goris, K. Devloo-Casier, E. Levrau, E. Biermans, M. R. Baklanov, K. F. Ludwig, P. V. D. Voort, S. Bals, C. Detavernier, *Chem. Mater.* **2012**, *24*, 1992 – 1994.

[33] a) I. Florea, A. Demortiere, C. Petit, H. Bulou, C. Hirlimann, O. Ersen, *ACS Nano* **2012**, *6*, 2574 – 2581; b) Z. Lu, Y. Yin, *Chem. Soc. Rev.* **2012**, *41*, 6874 – 6887; c) A. Sanchez-Iglesias, M. Grzelczak, T. Altantzis, B. Goris, J. Perez-Juste, S. Bals, G. Van Tendeloo, S. H. Donaldson, B. F. Chmelka, J. N. Israelachvili, L. M. Liz-Marzan, *ACS Nano* **2012**, *6*, 11059 – 11065.

[34] W. Van den Broek, A. Rosenauer, B. Goris, G. Martinez, S. Bals, S. Van Aert, D. Van Dyck, *Ultramicroscopy* **2012**, *116*, 8 – 12.

[35] T. Altantzis, B. Goris, A. Sanchez-Iglesias, M. Grzelczak, L. M. Liz-Marzan, S. Bals, *Part. Part. Syst. Charact.* **2013**, *30*, 84 – 88.

[36] a) P. Ercius, M. Weyland, D. A. Muller, L. M. Gignac, *Appl. Phys. Lett.* **2006**, *88*, 243116; b) H. L. L. Xin, Y. Zhu, D. A. Muller, *Microsc. Microanal.* **2012**, *18*, 720 – 727.

[37] J. E. Galvan-Moya, T. Altantzis, K. Nelissen, F. M. Peeters, M. Grzelczak, L. M. Liz-Marzan, S. Bals, G. Van Tendeloo, *ACS Nano* **2014**, *8*, 3869 – 3875

[38] M. B. Sadan, L. Houben, S. G. Wolf, A. Enyashin, G. Seifert, R. Tenne, K. Urban, *Nano Lett.* **2008**, *8*, 891 – 896.

[39] K. Batenburg, S. Bals, S. Van Aert, T. Roelandts, J. Sijbers, *Microsc. Microanal.* **2011**, *17*, 934 – 935.

[40] D. L. Donoho, *IEEE Trans. Inf. Theory* **2006**, *52*, 1289 – 1306.

[41] M. J. Hytch, E. Snoeck, R. Kilaas, *Ultramicroscopy* **1998**, *74*, 131 – 146.

[42] B. Goris, A. De Backer, S. Van Aert, S. Gómez-Graña, L. M. Liz-Marzán, G. Van Tendeloo, S. Bals, *Nano Lett.* **2013**, *13*, 4236 – 4241.

[43] K. Lepinay, F. Lorut, R. Pantel, T. Epicier, *Micron* **2013**, *47*, 43 – 49.

[44] P. Schlossmacher, D. O. Klenov, B. Freitag, H. S. Von Harrach, *Mater. Today* **2010**, *18*, 14 – 20.

  

[45] A. Genc, L. Kovarik, M. Gu, H. K. Cheng, P. Plachinda, L. Pullan, B. Freitag, C. M. Wang, *Ultramicroscopy* **2013**, *131*, 24 – 32.

[46] a) J. H. Hodak, A. Henglein, G. V. Hartland, *Pure Appl. Chem.* **2000**, *72*, 189 – 197; b) R. Ferrando, J. Jellinek, R. L. Johnston, *Chem. Rev.* **2008**, *108*, 845 – 910.

[47] a) E. Gonzalez, J. Arbiol, V. F. Puntes, *Science* **2011**, *334*, 1377 – 1380; b) B. Goris, P. Lakshminarayana, S. Bals, G. Van Tendeloo, L. M. Liz-Marzan, *Nano Lett.* **2014**, *14*, 3220 – 3226.

[48] J. Nelayah, M. Kociak, O. Stephan, F. J. G. de Abajo, M. Tence, L. Henrard, D. Taverna, I. Pastoriza-Santos, L. M. Liz-Marzan, C. Colliex, *Nat. Phys.* **2007**, *3*, 348 – 353.

[49] A. Horl, A. Trugler, U. Hohenester, *Phys. Rev. Lett.* **2013**, *111*, 076801.

[50] O. Nicoletti, F. de La Pena, R. K. Leary, D. J. Holland, C. Ducati, P. A. Midgley, *Nature* **2013**, *502*, 80 – 84.